Journal of Computational Applied Mechanics 2023, 54(4): 588-606

DOI: 10.22059/JCAMECH.2023.366508.889

RESEARCH PAPER

Analysis of the Bio-Thermoelasticity Response of Biological Tissues Subjected to Harmonic Heating Using a Refined Green–Lindsay Model

Ashraf M. Zenkour [a,b,*], Tariq Saeed [c], Khadijah M. Alnefaie [a,d]

[a] *Department of Mathematics, Faculty of Science, King Abdulaziz University, Jeddah 21589, Saudi Arabia*
[b] *Department of Mathematics, Faculty of Science, Kafrelsheikh University, Kafrelsheikh 33516, Egypt.*
[c] *Financial Mathematics and Actuarial Science (FMAS)-Research Group, Department of Mathematics, Faculty of Science, King Abdulaziz University, Jeddah 21589, Saudi Arabia.*
[d] *Department of Mathematics, Faculty of Science and Arts in Almakhwah, Albaha University, Almakhwah 65311, Saudi Arabia.*

Abstract

This study focuses on the analysis of the bio-thermoelasticity response exhibited by biological tissues when their inner and outer surfaces are free from stress and exposing the outer surface of the skin to harmonic heating with heatlessness of the inner surface of the skin. The investigation employs a refined Green–Lindsay model for a comprehensive understanding of the phenomenon. A system of partial differential equations is written and the solution is obtained using the Laplace transform and numerical inverse Laplace. The current model's results for temperature, displacement, stress, and strain distributions are presented, and it is compared to various (coupled and uncoupled) models from previous literature. The relaxation times effect on the model with other models is clarified, the effect of time, and some vital parameters are also studied, and tabularly to illustrate the effect of blood perfusion on the four distributions.

Keywords: Bio-thermoelasticity; classical coupled theory; Lord–Shulman theory; refined Green–Lindsay; Pennes' model; thermal wave theory; dual phase-lag theory; harmonic heating; skin tissue; Laplace transform.

1. Nomenclature

x, y, z	coordinate system
σ_{ij}	stress tensor (N m^{-2})
σ	normal stress (N m^{-2})
e_{ij}	strain tensor
e	dilatation
u_i	displacement components (mm)
∇^2	Laplacian operator
L	the thickness of the biological tissue (mm)
ω	angular frequency parameter (rad s^{-1})
t	time (s)
λ_t, μ_t	Lamé's constant of the skin tissue (kg m^{-1} s^{-2})
τ_1, τ_2	relaxation times (s)

* Corresponding author. *E-mail address:* zenkout@kau.edu.sa

Q	external heat source ($\mathrm{W\ m^{-3}}$)
ρ_t	the mass density of the skin tissue ($\mathrm{kg\ m^{-3}}$)
k_t	coefficient of thermal conductivity of skin tissue ($\mathrm{W\ m^{-1}\ K^{-1}}$)
c_t	specific heat capacity of the skin tissue ($\mathrm{J\ kg^{-1}\ K^{-1}}$)
α_t	thermal expansion coefficient ($\mathrm{K^{-1}}$)
γ_t	thermal modulus ($\mathrm{kg\ m^{-1}\ s^{-2}\ K^{-1}}$)
w_b	rate of blood perfusion ($\mathrm{s^{-1}}$)
ρ_b	the mass density of the blood ($\mathrm{kg\ m^{-3}}$)
c_b	specific heat capacity of the blood transverse ($\mathrm{J\ kg^{-1}\ K^{-1}}$)
T_b	reference temperature of the blood (K)
T	temperature distribution field (K)
$\theta = T - T_b$	temperature change (K)
Q_m	the heat source of metabolic generation of tissue cells ($\mathrm{Wm^{-3}}$)
Q_L	external thermal load ($\mathrm{Wm^{-3}}$)
s	Laplace parameter

2. Introduction

Heat treatments for diseased and injured skin tissues, such as skin cancer and skin burns, have recently been developed as a result of advancements in lasers, microwaves, and related technologies. Pre-infecting thermal harm within tissue structures a few millimeters below the surface is the goal, but it must be done without injuring nearby healthy tissue. The accuracy of the temperature, damage, and stress distributions in tissues must be predicted and controlled if these thermal therapies are to be effective. From a therapeutic perspective, high-intensity heating only lasts a short time.

Most biological heat transfer theories are generated according to the classical Fourier's law, which describes the propagation of a thermal signal very quickly. In the modern literature, a variety of biothermal transport theories have been developed for skin tissues, including models based on the uncoupled theory which are mainly based on the study of the heat conduction equation only while neglecting the mechanistic aspects such as Pennes' equation [1] which is used widely to model such problems due to its simplicity and assumes that the speed of thermal energy transfer is infinite, in fact heat propagates with finite speed.

By modifying the Fourier's rule of heat conduction, Cattaneo and Vernotte (C–V) [2, 3] independently suggested a modified constitutive relation to address this illogical behavior: The thermal wave (TW) theory where phase lag time captures the micro-scale responses in time due to heat flux. Also, one of those who modified Fourier's law to solve the issue of the infinite diffusion of heat is Tzou [4] who suggested the dual-phase-lag (DPL) theory.

Wahyudi and Gapsari [5] proposed a modification to the Pennes equation, which is commonly used to model heat transfer in human skin tissues. The modified equation was solved using the finite volume method (FVM). A study on bioheat transfer guided by the Pennes equation was presented by Sreegowrav et al [6]. Kaur et al. [7] evaluated the thermal damage in tissue caused by laser heating using a 1D bioheat model with a memory-dependent derivative (MDD) in Pennes' bioheat transfer equation. A unified system to represent some thermoelasticity models in general derived by Bera et al. [8] for isotropic and homogeneous thermoelastic solids. A study by Oguntala et al. [9]modeled the non-Fourier bioheat process in human skin using a multi-domain trivariate spectral collocation method to assess skin burn injuries.

In bioheat transfer, a one-dimensional, three-layer skin tissue model was used, and the TW was employed by Ozen et al. [10] as a technique in the heat analysis of tissues exposed to microwaves. A 2D single-phase-lag (SPL) bioheat transfer model was used by Abbas et al. [11] to study laser-irradiated biological tissues. The C-V equation took into account to describe the bioheat transfer in cylindrical skin tissue to determine the external heat flux and relaxation time based on 'measured' heating/cooling curves at several chosen places on the skin's surface by Mochnacki and Paruch [12].

Sharma and Kumar [13] employed the highly non-linear DPL bioheat transfer model to ascertain the significant contribution of hyperthermia treatment in the management of infected cells. Ziaeipoor et al. [14] concentrated on the temperature response of the skin tissue in response to time-dependent surface heat fluxes using a DPL model. Ezzat [15] developed a model based on the thermo-viscoelasticity theory of fractional DPL heat conduction equation with rheological features of the volume to investigate the bioheat transfer. The study conducted by Kumar et al. [16] focused on demonstrating the thermal damage caused to skin tissue when exposed to a heat source in motion and used the DPL model of bioheat transfer. Hu et al. [17] introduced a bioheat conduction model that incorporates a time-fractional DPL approach to analyze the thermoelastic response of skin when exposed to abrupt temperature changes. Zhou et al. [18] presented a DPL bioheat conduction model, together with the broad beam irradiation method, and rate process

equation to study thermal damage in laser-irradiated tissues.

Kumar et al. [19] constructed classical Fourier, SPL, and DPL models to study the phenomenon of bioheat transfer in various biological tissues. Kumar et al. [20] investigated tissue temperature-dependent thermal conductivity using Pennes' and TW equations. In their study, Fazlali and Ahmadikia [21] employed the TW and Pennes bioheat models within a setting of arbitrary periodic boundary conditions. The bioheat transfer equations of TW and DPL are analytically solved by Forghani et al. [22] considering the non-Fourier boundary conditions.

The bioheat transfer was also studied using models based on the coupled theory, which relies on the study of heat distribution, taking into account the mechanical aspects such as the classical coupled thermoelasticity theory (CTE) suggested by Biot [23], Lord–Shulman theory (L–S) [24], Green–Lindsay theory (G–L) [25], and Green–Naghdi theory (G–N) [26].

Bagri and Eslami [27] applied the G–L theory of thermoelasticity to analyze the thermoelastic behavior of graded hollow spheres and made a comparison with the results of CTE theory. Thermal shock response in a homogeneous porous orthotropic medium in the context of the G–L model of hyperbolic thermoelasticity has been investigated by Pramanik and Biswas [28]. The surface wave propagation in generalized magneto-thermoelastic materials taking the G–L model with voids and initial stress was investigated by Abo-Dahab [29]. Analyzed the effects of temperature-dependent thermal conductivity on thermoelastic interactions in a medium with a spherical cavity under two-temperature G–L theory by Kumar et al [30]. In the context of the modified G–L theory with strain rate dependence, Sarkar et al. [31] discussed the reflection and propagation of thermoelastic harmonic plane waves from the stress-free and isothermal surface of a homogeneous, isotropic thermally conducting elastic half-space.

Choudhuri [32] established a generalized mathematical model of a coupled thermoelasticity theory that includes three-phase-lag (TPL) that contains many theories of thermoelasticity. Hobiny et al. [33] proposed an analytical method for calculating thermal damages and temperature due to laser irradiation by using skin surface measurement data in the context of TPL. Zankour et al. [34] evaluated a new thermoelasticity model that included thermal conductivity applied in skin tissue. Fractional order theory with the fractional Caputo derivative and solutions for dimensionless temperature, displacement, stress, and strain in the current model shows that the fractional order parameter strongly affects distributions. Zenkour and his colleagues [35-37] studied the thermomechanical response of skin tissue in 1D under the influence of ramp-type heating using the refined L–S, G–L, and DPL models.

As a result of advancements and refinements in the field of thermodynamics and its application in the field of bio-mathematics, a novel and modified version of the G–L theory of thermoelasticity has been formulated [34-43]. The differential equations for the coupled thermoelastic system are established. The distributions of field quantities such as temperature, stress, displacement, and dilatation are examined. On thermoelastic behaviors, the possible effects of the G–L relaxation times and different variables are discussed. The objective of this research is to provide an improved version of the G–L thermoelasticity theory. This model will be employed to investigate the behavior of biological tissues, with a particular focus on analyzing the impact of applied convection.

3. Formulation of the problem

Assume that the thinner one-dimensional skin tissue has a thickness of L mm, such that the outer surface of the biological tissue is traction-free and subjected to the applied convection effect (harmonic heating). In addition, its inner surface should be traction-free and without any temperature increment (see Figure 1).

The following refined G–L theory of thermoelasticity, which includes the CTE theory, the L–S, and the simple G–L theory. The general formula of the heat conduction equation can be expressed as [34-42]

$$k_t\left[\epsilon_1+\sum_{n=1}^{N}\frac{\tau_2^{n-1}}{(n-1)!}\frac{\partial^{n-1}}{\partial t^{n-1}}\right]\nabla^2\theta=\rho_t c_t\left(1+\sum_{n=1}^{N}\frac{\tau_1^{n}}{n!}\frac{\partial^{n}}{\partial t^{n}}\right)\frac{\partial\theta}{\partial t}+\left[\epsilon_2+\sum_{m=1}^{M}\frac{\tau_1^{m-1}}{(m-1)!}\frac{\partial^{m-1}}{\partial t^{m-1}}\right]\left(\gamma_t T_b\frac{\partial e}{\partial t}-Q\right), \quad (1)$$

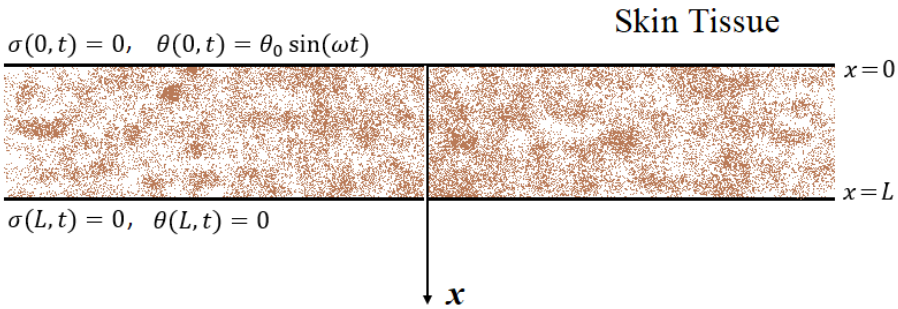

Fig. 1: The one-dimensional skin tissue model with boundary conditions

where ϵ_1, and ϵ_1 are parameters may be one or zero and $N, M \geq 1$.

The constitutive relation is also modified along the same lines as the G–L model as

$$\sigma_{ij} = \lambda_t e_{kk}\delta_{ij} + 2\mu_t e_{ij} - \gamma_t \left(1 + \sum_{n=1}^{N} \frac{\tau_2^n}{n!}\frac{\partial^n}{\partial t^n}\right)\theta\delta_{ij}, \tag{2}$$

and then the equation of motion in terms of displacement will be reduced to

$$\mu_t u_{i,jj} + (\lambda_t + \mu_t)u_{k,ki} - \gamma_t \left(1 + \sum_{n=1}^{N} \frac{\tau_2^n}{n!}\frac{\partial^n}{\partial t^n}\right)\theta_{,i} + \rho_t f_i = \rho_t \ddot{u}_i, \tag{3}$$

where $i, j, k = x, y, z$. According to the hypothesis that the problem is in one dimension, then the displacement components are as follows

$$u_x = u(x,t), \qquad u_y = u_z = 0, \tag{4}$$

the strain-displacement field can be displayed as

$$e_{ij} = \frac{1}{2}\left(u_{i,j} + u_{j,i}\right), \tag{5}$$

$$e_{yz} = e_{xz} = e_{xy} = e_{yy} = e_{zz} = 0, \tag{6}$$

and

$$e_{xx} = \frac{\partial u}{\partial x}. \tag{7}$$

So, from Eqs. (2) and (6) the stress components become

$$\sigma_{yz} = \sigma_{xz} = \sigma_{xy} = \sigma_{yy} = \sigma_{zz} = 0, \tag{8}$$

and

$$\sigma_{xx} = (\lambda_t + 2\mu_t)e_{xx} - \gamma_t \left(1 + \sum_{n=1}^{N} \frac{\tau_2^n}{n!}\frac{\partial^n}{\partial t^n}\right)\theta. \tag{9}$$

For simplicity $u_x = u$, $e_{xx} = e$, $\sigma_{xx} = \sigma$, then the equation of motion where no external forces are affecting the skin

$$(\lambda_t + 2\mu_t)\frac{\partial^2 u}{\partial x^2} - \gamma_t \left(1 + \sum_{n=1}^{N} \frac{\tau_2^n}{n!}\frac{\partial^n}{\partial t^n}\right)\frac{\partial \theta}{\partial x} = \rho_t \frac{\partial^2 u}{\partial t^2}. \tag{10}$$

From this model in Eqs. (1) and (3), many theories of thermoelasticity can be obtained as follows

- The CTE theory where $\tau_1 = \tau_2 = 0$, $\epsilon_1 = \epsilon_2 = 1$.
- The L–S theory where $\tau_2 = 0$, $N = 1$, $M = 2$, $\epsilon_1 = 1$, $\epsilon_2 = 0$.
- The simple G–L theory is obtained by $\epsilon_1 = \epsilon_2 = 0$, $N = M = 1$.

4. The governing system

As a consequence of numerous studies, the external heat source can be determined to study the bio-thermoelastic response of biological tissues by the relation

$$Q = w_b \rho_b c_b (T_b - T) + Q_m + Q_L. \tag{11}$$

Thus, the heat conduction equation of refined G–L theory for skin tissues becomes as follows

$$k_t\left[\epsilon_1+\sum_{n=1}^{N}\frac{\tau_2^{n-1}}{(n-1)!}\frac{\partial^{n-1}}{\partial t^{n-1}}\right]\left(\frac{\partial^2\theta}{\partial x^2}\right)=\rho_t c_t\left(1+\sum_{n=1}^{N}\frac{\tau_1^n}{n!}\frac{\partial^n}{\partial t^n}\right)\frac{\partial\theta}{\partial t}+$$

$$+\left[\epsilon_2+\sum_{m=1}^{M}\frac{\tau_1^{m-1}}{(m-1)!}\frac{\partial^{m-1}}{\partial t^{m-1}}\right]\left(\gamma_t T_b\frac{\partial e}{\partial t}+w_b\rho_b c_b\theta-Q_m-Q_L\right),\quad N\geq 1, M\geq 1. \tag{12}$$

Suppose that the initial conditions of the tissue examined are homogeneous since there is no heat or displacement in the biological tissue at the beginning of time

$$\begin{aligned}u(x,t)|_{t=0}&=\left.\frac{\partial^n u(x,t)}{\partial t^n}\right|_{t=0}=0\\ \theta(x,t)|_{t=0}&=\left.\frac{\partial^n \theta(x,t)}{\partial t^n}\right|_{t=0}=0\end{aligned},\quad n\geq 1. \tag{13}$$

To determine the boundary conditions of the problem, suppose that the inner and outer surfaces of the biological tissues are not subjected to any kind of stress, that means

$$\sigma(0,t)=0,\quad \sigma(L,t)=0, \tag{14}$$

and that the tissue is only subjected to harmonic heating at the beginning of tissue, whereas no temperature exists on the plane $x=L$

$$\theta(0,t)=\theta_0\, sin(\omega t),\quad t\geq 0,\quad \theta(L,t)=0. \tag{15}$$

To treat the problem, consider the refined G–L model, dividing both sides of Eq. (12) by $\rho_t c_t$ with $Q_L=0$, hence it gets

$$C_T^2\left(\epsilon_1+\sum_{n=1}^{N}\frac{\tau_2^{n-1}}{(n-1)!}\frac{\partial^{n-1}}{\partial t^{n-1}}\right)\left(\frac{\partial^2\theta}{\partial x^2}\right)=\left(1+\sum_{n=1}^{N}\frac{\tau_1^n}{n!}\frac{\partial^n}{\partial t^n}\right)\frac{\partial\theta}{\partial t}+$$

$$+\left(\epsilon_2+\sum_{m=1}^{M}\frac{\tau_1^{m-1}}{(m-1)!}\frac{\partial^{m-1}}{\partial t^{m-1}}\right)\left(\eta\frac{\partial^2 u}{\partial t\partial x}+w_b\rho_c\theta-Q_0\right), \tag{16}$$

where

$$C_T^2=\frac{k_t}{\rho_t c_t},\quad \eta=\frac{\gamma_t T_b}{\rho_t c_t},\quad \rho_c=\frac{\rho_b c_b}{\rho_t c_t},\quad Q_0=\frac{Q_m}{\rho_t c_t}. \tag{17}$$

In Eq. (10), dividing both sides by $\lambda_t+2\mu_t$ to get

$$\frac{\partial^2 u}{\partial x^2}-c_1\left(1+\sum_{n=1}^{N}\frac{\tau_2^n}{n!}\frac{\partial^n}{\partial t^n}\right)\frac{\partial\theta}{\partial x}=\frac{1}{C_p^2}\frac{\partial^2 u}{\partial t^2}, \tag{18}$$

where

$$c_1=\frac{\gamma_t}{\lambda_t+2\mu_t},\quad C_p^2=\frac{\lambda_t+2\mu_t}{\rho_t}. \tag{19}$$

Equation (9) also by dividing both sides by $\lambda_t+2\mu_t$ gives

$$\frac{\sigma}{\lambda_t+2\mu_t}=\frac{\partial u}{\partial x}-c_1\left(1+\sum_{n=1}^{N}\frac{\tau_2^n}{n!}\frac{\partial^n}{\partial t^n}\right)\theta. \tag{20}$$

5. Solution of the problem

To obtain a solution to the coupled problem between heat and motion and to obtain the numerical quantities of temperature, displacement, stress, and dilatation, the Laplace transform will be applied to the system of Eqs. (16), (18), and (20) to transform it from a system of partial differential equations that are difficult to solve into a system of ordinary differential equations that can be solved, the Laplace transform characterized by

$$\bar{f}(x,s) = \int_0^\infty e^{-st} f(x,t)dt. \tag{21}$$

Apply the Laplace transform to Eq. (18), and using the initial conditions Eq. (13)

$$\frac{d^2\bar{u}}{dx^2} - c_1\left(1 + \sum_{n=1}^{N} \frac{\tau_2^n}{n!} s^n\right) = \frac{1}{C_p^2} s^2 \bar{u}, \tag{22}$$

it is important to remember that the over-bar image signifies the Laplace transform,

$$\left(\frac{d^2}{dx^2} - 2c_3\right)\bar{u} = c_2 \frac{d\bar{\theta}}{dx}, \tag{23}$$

where

$$c_2 = c_1\left(1 + \sum_{n=1}^{N} \frac{\tau_2^n}{n!} s^n\right), \quad c_3 = \frac{s^2}{2C_P^2}. \tag{24}$$

Again, applying the Laplace transform in Eq. (16) and using the initial conditions in Eq. (13)

$$C_T^2\left[\epsilon_1 + \sum_{n=1}^{N} \frac{\tau_2^{n-1}}{(n-1)!} s^{n-1}\right]\frac{d^2\bar{\theta}}{dx^2} = \left[s\left(1 + \sum_{n=1}^{N} \frac{\tau_1^n}{n!} s^n\right) +\right.$$

$$\left. + w_b\rho_c\left(\epsilon_2 + \sum_{m=1}^{M} \frac{\tau_1^{m-1}}{(m-1)!} s^{m-1}\right)\right]\bar{\theta} + \eta s\left[\epsilon_2 + \sum_{m=1}^{M} \frac{\tau_1^{m-1}}{(m-1)!} s^{m-1}\right]\frac{d\bar{u}}{dx} - Q_0. \tag{25}$$

Let

$$c_4 = \frac{1}{2C_T^2\left[\epsilon_1 + \sum_{n=1}^{N} \frac{\tau_2^{n-1}}{(n-1)!} s^{n-1}\right]}\left[s\left(1 + \sum_{n=1}^{N} \frac{\tau_1^n}{n!} s^n\right) + w_b\rho_c(\epsilon_2 + \sum_{m=1}^{M} \frac{\tau_1^{m-1}}{(m-1)!} s^{m-1})\right],$$

$$c_5 = \frac{\eta s\left[\epsilon_2 + \sum_{m=1}^{M} \frac{\tau_1^{m-1}}{(m-1)!} s^{m-1}\right]}{2C_T^2\left[\epsilon_1 + \sum_{n=1}^{N} \frac{\tau_2^{n-1}}{(n-1)!} s^{n-1}\right]}, \quad Q_1 = \frac{Q_0}{sC_T^2\left[\epsilon_1 + \sum_{n=1}^{N} \frac{\tau_2^{n-1}}{(n-1)!} s^{n-1}\right]}, \tag{26}$$

then

$$\left(\frac{d^2}{dx^2} - 2c_4\right)\bar{\theta} = 2c_5 \frac{d\bar{u}}{dx} - Q_1. \tag{27}$$

Once more, taking the Laplace transform of both sides of Eq. (20) and using initial conditions by Eq. (13), then

$$\frac{\bar{\sigma}}{\lambda_t + 2\mu_t} = \frac{d\bar{u}}{dx} - c_2\bar{\theta}. \tag{28}$$

Laplace transform for boundary conditions

$$\bar{\sigma}(0,s) = 0, \quad \bar{\sigma}(L,s) = 0, \quad \bar{\theta}(0,s) = \theta_0 \frac{\omega}{s^2 + \omega^2}, \quad \bar{\theta}(L,s) = 0. \tag{29}$$

By solving the system of equations shown in Eqs. (23) and (27) in the Laplace field to obtain the solution as

$$\bar{\theta} = \sum_{i=1}^{2}\left(A_i\, e^{\xi_i x} + B_i\, e^{-\xi_i x}\right) + Q_2, \tag{30}$$

$$\bar{u} = \sum_{i=1}^{2} \beta_i\left(A_i\, e^{\xi_i x} - B_i\, e^{-\xi_i x}\right), \tag{31}$$

where

$$\xi_1, \xi_2 = \sqrt{c_2 c_5 + c_3 + c_4 \pm \xi_0}, \quad Q_2 = \frac{Q_1}{2c_4},$$

$$\xi_0 = \sqrt{(c_2 c_5 + c_3)^2 + c_4[c_4 + 2(c_2 c_5 - c_3)]},$$

$$\beta_i = \frac{\xi_i(\xi_i^2 - 2c_2 c_5 - 2c_4)}{4c_3 c_5}, \tag{32}$$

where A_i and B_i are constant coefficients that vary with s.

Moreover, the dilatation is given in the Laplace domain

$$\bar{e} = \sum_{i=1}^{2} \beta_i \xi_i \left(A_i\, e^{\xi_i x} + B_i\, e^{-\xi_i x}\right). \tag{33}$$

Substituting from Eqs. (30) and (31) in Eq. (28), thus the stress will be in the form

$$\bar{\sigma} = \sum_{i=1}^{2} \zeta_i \left(A_i\, e^{\xi_i x} + B_i\, e^{-\xi_i x}\right) - Q_3, \tag{34}$$

where

$$\zeta_i = \beta_i \xi_i (\lambda_t + 2\mu_t) - \gamma_t \left(1 + \sum_{n=1}^{N} \frac{\tau_2^n}{n!} s^n\right), \quad Q_3 = \gamma_t \left(1 + \sum_{n=1}^{N} \frac{\tau_2^n}{n!} s^n\right) Q_2. \tag{35}$$

The solution to the overflowing arrangement of direct conditions provides the unknown parameters A_i and B_i. By using Eqs. (30), (34), and (29), and applying the above boundary conditions, one obtains

$$\begin{bmatrix} 1 & 1 & 1 & 1 \\ e^{\xi_1 L} & e^{-\xi_1 L} & e^{\xi_2 L} & e^{-\xi_2 L} \\ \zeta_1 & \zeta_1 & \zeta_2 & \zeta_2 \\ \zeta_1 e^{\xi_1 L} & \zeta_1 e^{-\xi_1 L} & \zeta_2 e^{\xi_2 L} & \zeta_2 e^{-\xi_2 L} \end{bmatrix} \begin{Bmatrix} A_1 \\ B_1 \\ A_2 \\ B_2 \end{Bmatrix} = \begin{Bmatrix} \frac{\omega \theta_0}{s^2 + \omega^2} - Q_2 \\ -Q_2 \\ Q_3 \\ Q_3 \end{Bmatrix}. \tag{36}$$

For the solution to be complete in the domain of the Laplace transform, the preceding system of linear equations is solved to get the following parameters

$$A_1 = \frac{(Q_2\zeta_2 + Q_3)e^{\xi_1 L} - \left[\left(Q_2 - \theta_0 \frac{\omega}{s^2+\omega^2}\right)\zeta_2 + Q_3\right]}{(\zeta_1 - \zeta_2)(e^{2\xi_1 L} - 1)}, \tag{37}$$

$$B_1 = \frac{-\left\{Q_2\zeta_2 + Q_3 - \left[\left(Q_2 - \theta_0 \frac{\omega}{s^2+\omega^2}\right)\zeta_2 + Q_3\right]e^{\xi_1 L}\right\}e^{\xi_1 L}}{(\zeta_1 - \zeta_2)(e^{2\xi_1 L} - 1)}, \tag{38}$$

$$A_2 = \frac{-(Q_2\zeta_1 + Q_3)e^{\xi_2 L} + \left(Q_2 - \theta_0 \frac{\omega}{s^2+\omega^2}\right)\zeta_1 + Q_3}{(\zeta_1 - \zeta_2)(e^{2\xi_2 L} - 1)}, \tag{39}$$

$$B_2 = \frac{\left\{Q_2\zeta_1 + Q_3 - \left[\left(Q_2 - \theta_0 \frac{\omega}{s^2+\omega^2}\right)\zeta_1 + Q_3\right]e^{\xi_2 L}\right\}e^{\xi_2 L}}{(\zeta_1 - \zeta_2)(e^{2\xi_2 L} - 1)}. \tag{40}$$

The transform domain problem has now been completely resolved. Due to the complexity of the formulations in Eqs. (30) and (31), achieving the inverse transform in the time domain analytically is relatively difficult. As a result, the numerical inverse Laplace transform technique will be used to determine the impacts on temperature θ, displacement u, strain e, and stress σ in the real-time domain. To obtain numerical results in the physical domain, the Riemann-sum approximation method can be employed. Every function $\bar{f}(x,s)$ in the Laplace transform space is translated into a physical domain $f(x,t)$ in this manner by utilizing the famous equation [44, 45]

$$f(x,t) = \frac{e^{\varrho t}}{t}\left[\frac{1}{2} Re\{\bar{f}(x,\varrho)\} + Re\left\{\sum_{r=0}^{R}\left(\bar{f}\left(x, \varrho + \frac{ir\pi}{t}\right)(-1)^r\right)\right\}\right], \tag{41}$$

where Re denotes a function's real part, $r \in N$, and $\mathrm{i} = \sqrt{-1}$ and $\varrho \approx 4.7/t$ [45].

6. Numerical results

To display the numerical results of temperature θ, displacement u, dilatation e, and stress σ under harmonic heating on the surface of the skin tissue have thickness $L = 1$ mm, $\theta_0 = 80$ K, and $N = M = 3$, and the following constants are used.

Table 1: Elastic constants of skin biological tissue and blood.

Property	Value
λ_t	8.27×10^8
μ_t	3.446×10^7
c_t	3600
α_t	1×10^{-4}
γ_t	$(2\mu_t + 3\lambda_t)\alpha_t$
ρ_t	1190
k_t	0.235
ρ_b	1060
c_b	3770
w_b	0.00187
T_b	310
Q_m	368.1

Convection, as it relates to the harmonic heating burden on tissue, will be covered in this section. To validate the results of the new model's predictions and the scope of its applicability, the values of the four variables (temperature θ, displacement u, strain e, and stress σ) arising from the refined G–L model with time derivatives of order three will first be compared with those of their equivalents in three fundamental coupled and uncoupled thermoelasticity models of bioheat transfer, noting that the following values are used, the angular frequency parameter $\omega = 0.9$ rad s^{-1}, the time $t = 10$ s, and the relaxation times are $\tau_1 = 0.1$ s, $\tau_2 = 0.14$ s.

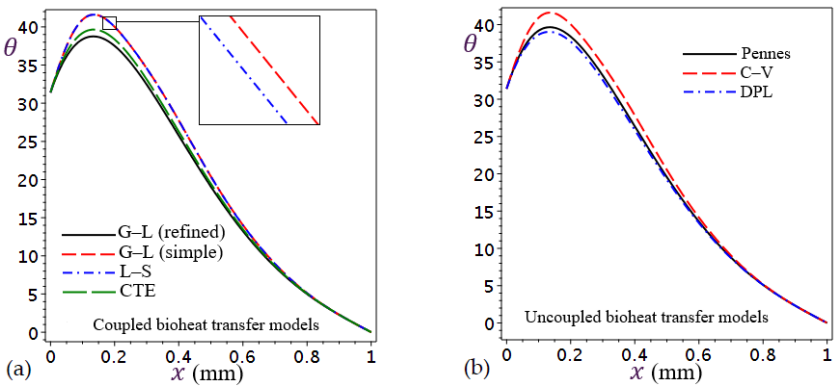

Fig. 2: 2D plots of different thermoelasticity theories, (a) temperature θ distributions in coupled models, (b) temperature θ distributions in uncoupled models.

As shown in Fig. 2, a comparison of the temperature distributions in the different models is shown. It is evident that the thermal behavior resulting from the use of the Pennes' model closely resembles that of the CTE model, a similarity also observed in the C–V and L–S models. The temperature θ distributions show that the temperature θ curve in the refined G–L theory follows the same behavior as the classical theories of thermoelasticity, where all the temperature θ distributions start from the same point at the edge of the skin and then the temperature rises through the depth of the tissue until it reaches its highest values at the position $x = 0.15$ mm, then it starts to descend until it reaches zero at the end of the biological tissue, thus achieving the boundary condition of the problem, the refined G–L theory gave the least temperature θ curve followed by the CTE theory and then the temperature θ distribution in the L–S theory approach to the temperature θ distribution in the simple G–L theory, and when zoomed in, it found that simple G–L theory gave a higher temperature at all.

To clarify the differences between the different theories and their effect on temperature, Table 2 presents the temperature distributions in three positions along the biological tissue $x = 0.1, 0.5, 0.9$ mm. At $x = 0.1$, the coupled theories give a higher temperature compared to their uncoupled theories counterparts, and with increasing depth, the opposite happens. The refined G–L theory of order 3 recorded the lowest temperature at all locations.

Table 2: Temperature θ distributions observed at various places under different thermoelasticity models elastic constants.

x(mm)	Pennes	CTE	C–V	L–S	DPL	Simple G–L	Refined G–L	
						$N = 1$	$N = 2$	$N = 3$
0.1	39.196528	39.200112	40.941968	40.947226	37.888769	40.951150	38.662772	38.379469
0.5	19.554126	19.454862	20.526712	20.413305	18.7642901	20.418548	19.159487	19.076184
0.9	2.322900	2.290969	2.328081	2.291099	2.342097	2.292293	2.323554	2.275442

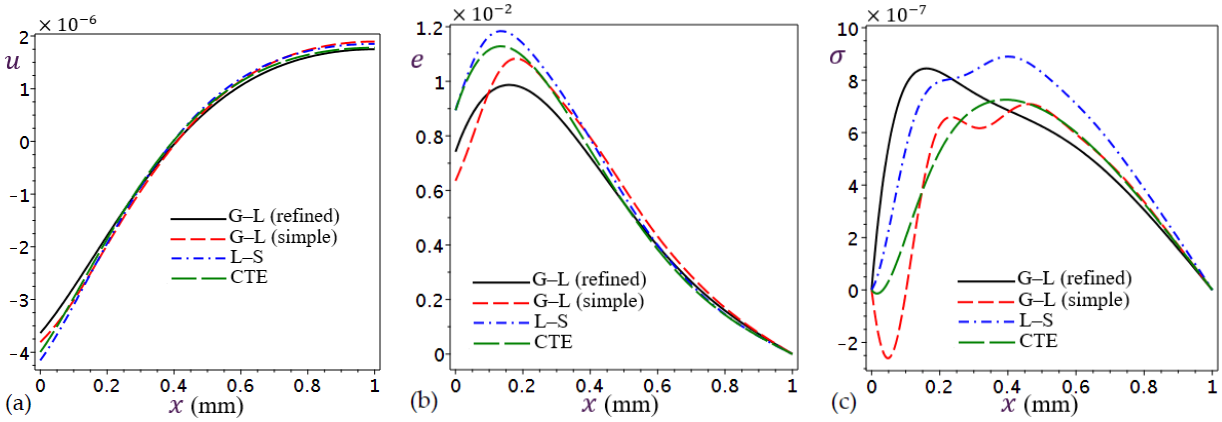

Fig. 3: 2D plots of different coupled thermoelasticity theories (a) displacement u distributions, (b) dilatation e distributions, and (c) stress σ distributions.

It is noted that the different distributions of displacement u in Fig. 3 are very close to each other and there is no difference in the general behavior of the curves as the displacement increases with increasing depth. The refined G–L theory gives a higher displacement curve than the other models until position $x = 0.3$ mm, after which the situation changes and the displacement generated by the refined G–L model becomes the lowest.

As for the dilatation e distributions, it is found that the lowest value of e resulting from the simple G–L theory up to $x = 0.1$ mm, after that, the distribution of e resulting from the refined G–L theory is the lowest until $x = 0.4$ mm then different curves approach each other until reach to zero.

For the stress σ distribution resulting from the refined G–L theory, it increases with increasing skin depth until it reaches the highest value at $x = 0.16$ mm and then decreases until it reaches zero at $x = L$ mm. In the CTE theory and the simple G–L theory, it takes negative values and then increases again until it reaches zero.

To characterize the temperature θ, displacement u, dilatation e, and stress σ distributions in the four theories and ascertain the impact of the angular frequency parameter, four different values of the angular frequency parameter are chosen, and the time is fixed $t = 10$ s and $\tau_1 = 0.1$ s, $\tau_2 = 0.14$ s. The results are presented in Figs. 4-7.

The effect of changing the values of the angular frequency parameter ω appears clear on the different temperature θ distributions, where the smaller ω values give higher temperature curves with the different behavior of the curve depending on the change in ω values, as described in Fig. 4. The distributions of θ in the refined G–L theory are affected similarly to the temperature θ distributions in the CTE theory. While the temperature θ curves in simple G–L theory and L–S theory are similar in behavior and response to change in ω. This is due to the similarity in the two theories to the common denominator between them in the effect on temperature in the heat conduction equation by adding a relaxation time with a first-order time derivative.

The displacement u distributions in the four models showed similar behavior when changing the values of the angular frequency parameter, with some minor differences in each model at the two edges of the biological tissue, as shown in Fig. 5.

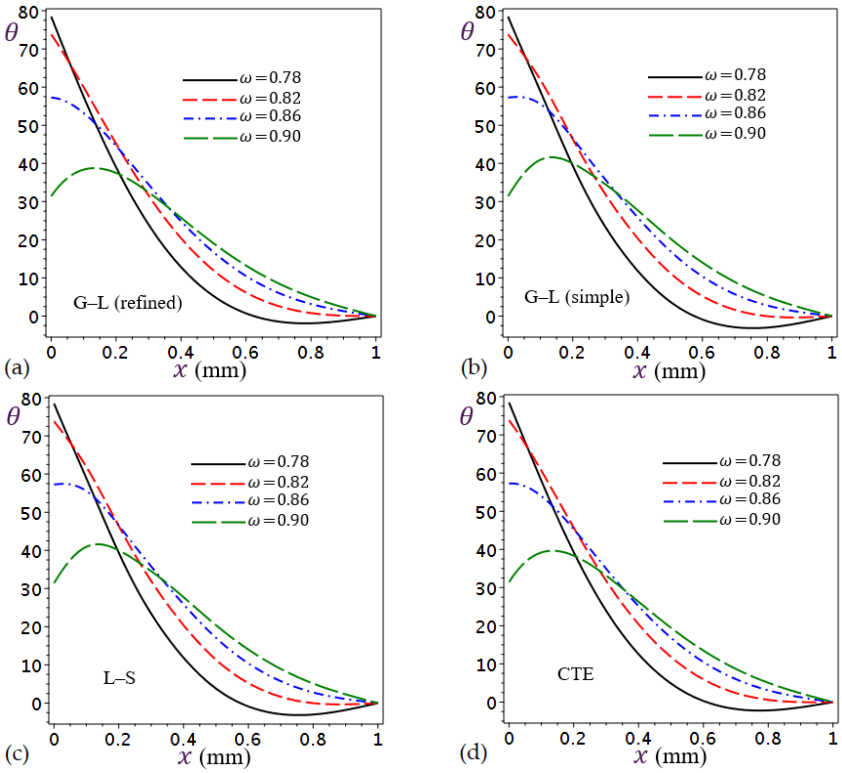

Fig. 4: Effect of angular frequency parameter ω on temperature θ (a) refined G–L theory, (b) simple G–L theory, (c) L–S theory, and (d) CTE theory.

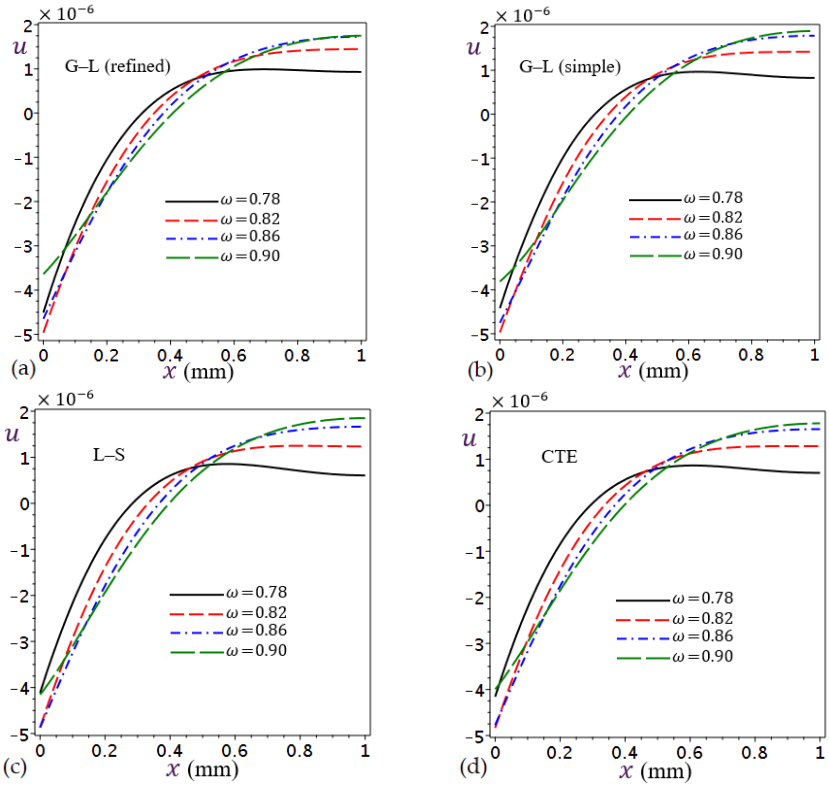

Fig. 5: Effect of angular frequency parameter ω on displacement u (a) refined G–L theory, (b) simple G–L theory, (c) L–S theory, and (d) CTE theory.

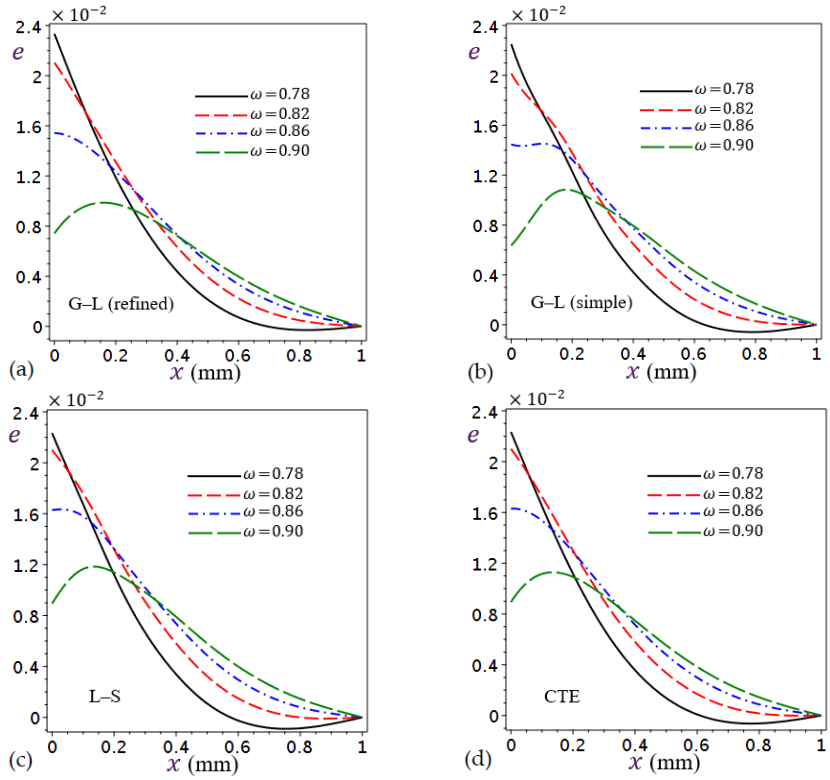

Fig. 6: Effect of angular frequency parameter ω on dilatation e (a) refined G–L theory, (b) simple G–L theory, (c) L–S theory, and (d) CTE theory.

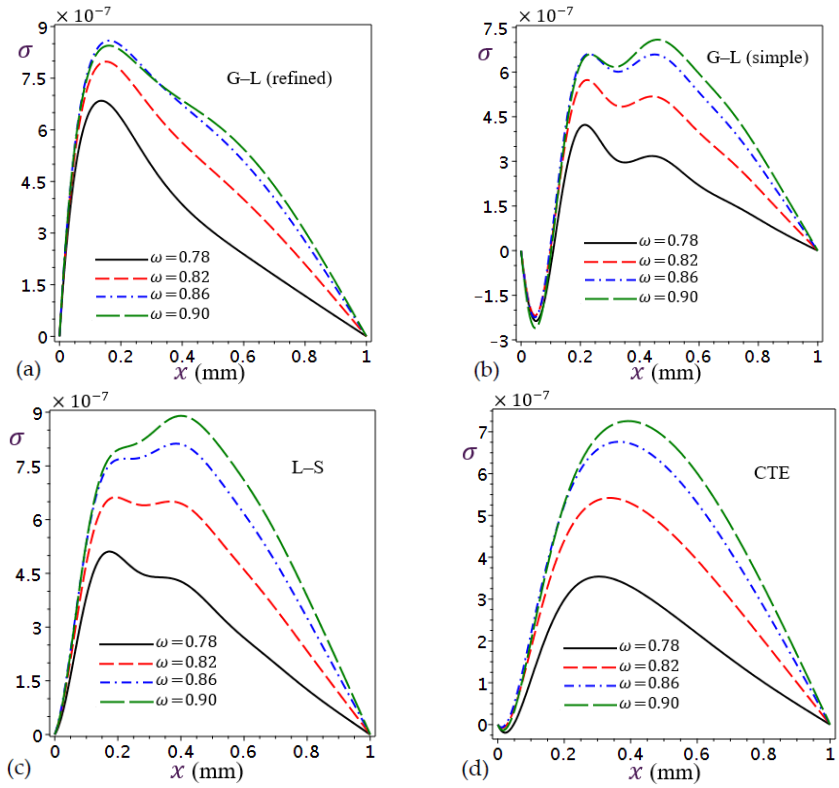

Fig. 7: Effect of angular frequency parameter ω on normal stress σ (a) refined G–L theory, (b) simple G–L theory, (c) L–S theory, and (d) CTE theory.

The dilatation e distributions in the simple G–L theory showed a different behavior from the other three models at the beginning of the biological tissue, while the response of the dilatation e distributions to the change in ω values in the refined G–L theory is similar to that of the CTE theory and the L–S theory as in Fig. 6.

The effect of the angular frequency coefficient ω on stress σ is shown in different theories of thermoelasticity as in Fig. 7, and it turns out that its effect is similar in the four models as higher ω values give higher stress σ curves while the distribution curves maintain the boundary conditions of the case, noting that greater ω, the closer the curves are to each other, with the difference in stress resulting from the refined G–L theory which showed the curve did not maintain its shape but rather changed at largest ω.

As depicted in Figs. 8-11, the second relaxation time is fixed at $\tau_2 = 0.25$ s, $t = 10$ s, and $\omega = 0.9$ rad s^{-1} while four various values for the first relaxation time τ_1 are examined for their effects.

Figure 8 shows the effect of the first relaxation time τ_1 on the temperature θ distributions in the refined G–L theory, the simple G–L theory, and the L–S theory. It is noted that the effect appears clear at the beginning of the biological tissue and decreases with the thickness of the skin until it vanishes at $x = L$ mm. It can be seen that the distributions of θ in the three models are affected by changing the first relaxation time in the same way, where higher τ_1 values give higher temperature curves. The effect in the refined G–L theory is slightly different in behavior than in the simple G–L theory and the L–S theory for temperature distributions.

As for the displacement u distributions shown in Fig. 9, the displacement in the refined G–L theory is affected by changing the different values of τ_1, especially at the larger values of τ_1, unlike the displacement in the simple G–L theory, the effect is regular and clear at both ends of the biological tissue and almost faded in the middle, this description also applies to displacement in the L–S theory with the difference being that the displacement curves are less affected by changing τ_1, values than the previous two models.

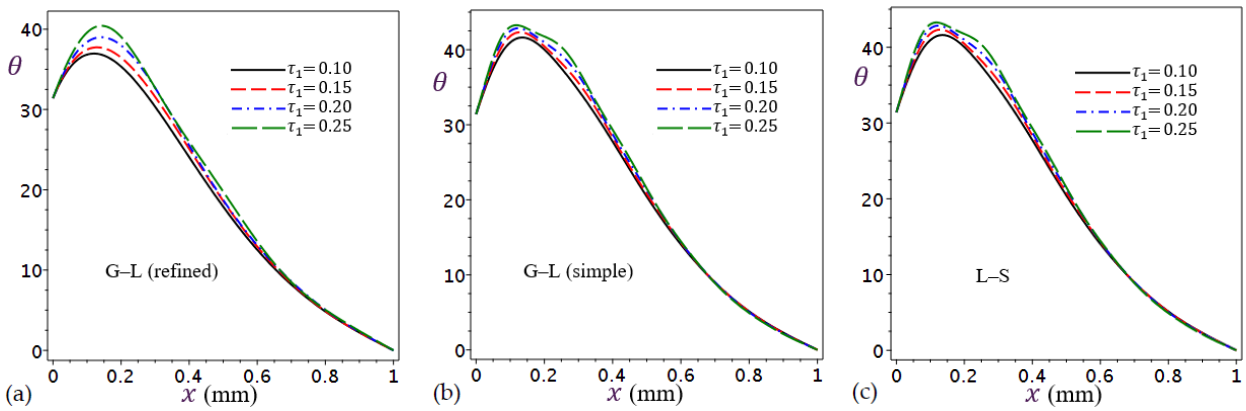

Fig. 8: Effect of first relaxation time τ_1 on temperature θ under harmonic heating (a) refined G–L theory, (b) simple G–L theory, and (c) L–S theory.

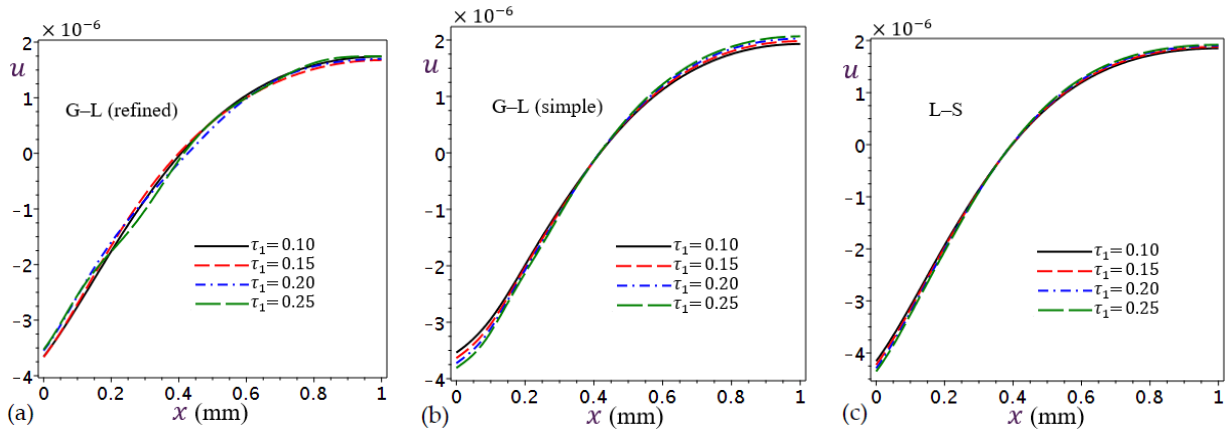

Fig. 9: Effect of first relaxation time τ_1 on displacement u under harmonic heating (a) refined G–L theory, (b) simple G–L theory, and (c) L–S theory.

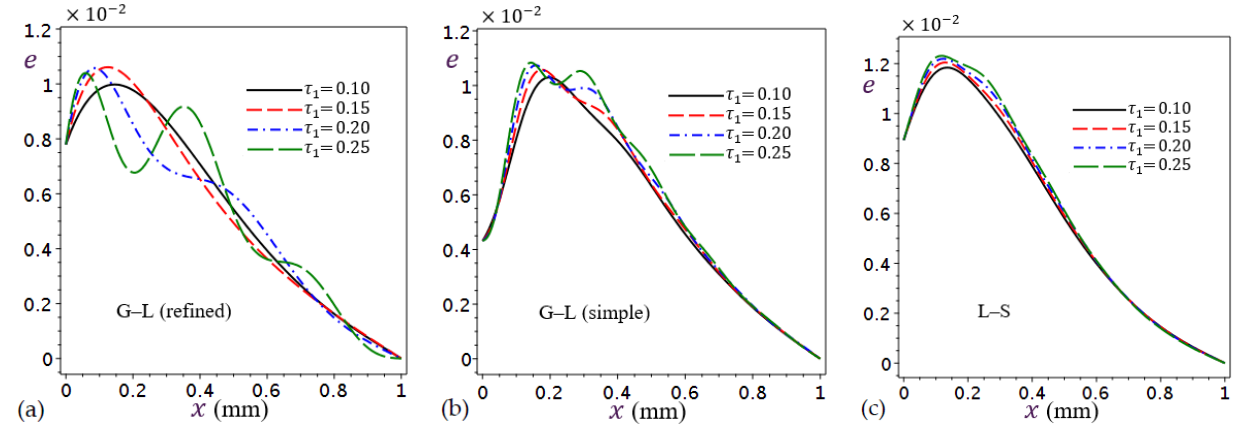

Fig. 10: Effect of first relaxation time τ_1 on dilatation e under harmonic heating (a) refined G–L theory, (b) simple G–L theory, and (c) L–S theory.

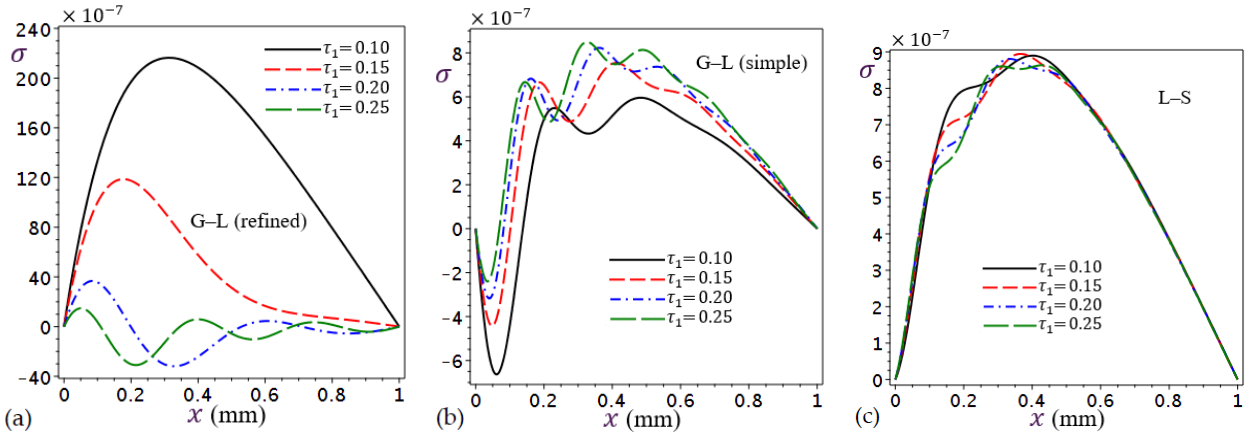

Fig. 11: Effect of first relaxation time τ_1 on normal stress σ under harmonic heating (a) refined G–L theory, (b) simple G–L theory, and (c) L–S theory.

The dilatation e distributions in the refined G–L theory are affected by the increase in the values of τ_1, as the higher the values, the curve becomes more wavy, as shown in Fig. 10. The same behavior appears in the dilatation curves in the simple G–L theory, but in a weaker way than the previous one, while the dilatation distributions shown in the L–S theory similar effect on temperature distributions for the same theory (see Fig. 8).

Figure 11 shows the different stress σ distributions. The effect of the change in the values of the first relaxation time is large and clear in the refined G–L theory, as the lowest value of τ_1 gave the largest stress curve, and as the values of τ_1 increased, the stress curve went down with an increase in ripple. As for the effect in the simple G–L theory, the stress curves maintained the unified shape and are affected by the increase and decrease according to changing the values of τ_1, while the stress curves in the L–S theory are affected very weakly and it is hardly clear except between the two positions $x = 0.1$ mm and $x = 0.5$ mm.

To investigate the effect of the second relaxation time of G–L, the first relaxation time is fixed by $\tau_1 = 0.1$ s, the time $t = 10$ s, $\omega = 0.9$ rad s^{-1}, and assigned four different values the second time, as shown in Figs. 12-15.

Figure 12 shows the clear effect of the second relaxation time τ_2 on the temperature θ distributions in the refined G–L theory, where the temperature decreases as the value of τ_2 increases, while the effect seems weak on the distributions of θ in the simple G–L theory, but when enlarged, the effect is that the larger the value of τ_2, the higher the temperature.

Figure 13 shows the effect of the second relaxation time τ_2 values on displacement u appear clearer in the refined G–L theory than in the simple G–L theory, where at the beginning of the tissue the displacement curves resulting from the largest $\tau_2$values are the least until the position $x = 0.43$ where all curves intersect and the effect of τ_2 fades at this point after which it is reflected so the higher displacement curves are those resulting from larger τ_2 values. As for the

simple G–L theory, the displacement at the beginning of the biological tissue, it found that the larger τ_2 values gave a higher displacement until the curves approached each other with the increase in skin thickness.

Figure 14 shows the distributions of the dilatation e increasing with the increase in the value of τ_2 in the refined G–L theory. It is also evident that the difference between the curves increases accordingly. As for its counterpart in the simple G–L theory, the opposite occurs, and it is seen that the largest dilatation curve is that resulting from the lower values of τ_2 from the beginning of the biological tissue to the point $x = 0.37$ mm, where the curves intersect and invert, and it gets higher dilatation curves than the larger τ_2 values.

The stress σ distributions also increase due to the increase in the values of τ_2 in refined G–L theory noticeably, as shown in Fig. 15. Contrary to what happened in the simple G–L theory, the distance between the curves is almost the same, and the increase in the values of τ_2 gave fewer stress curves.

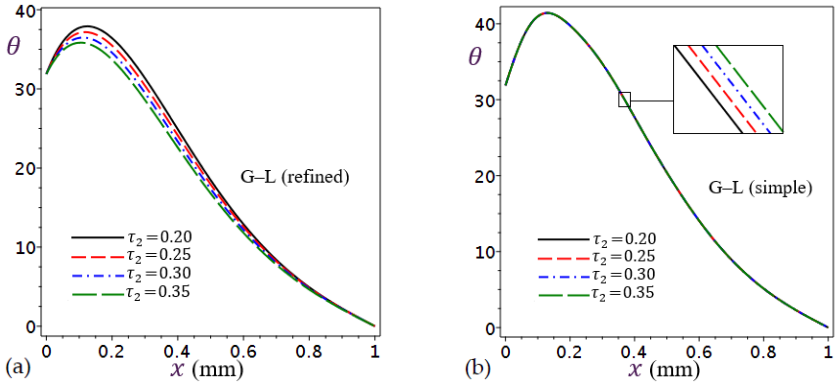

Fig. 12: Effect of second relaxation time τ_2 on temperature θ under harmonic heating (a) refined G–L theory and (b) simple G–L theory.

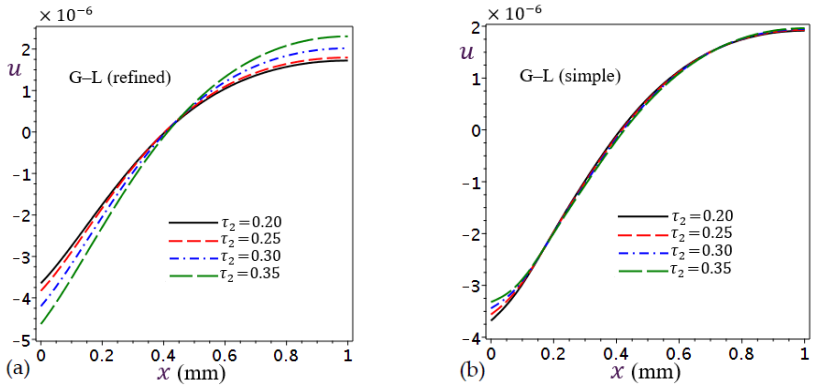

Fig. 13: Effect of second relaxation time τ_2 on displacement u under harmonic heating (a) refined G–L theory and (b) simple G–L theory.

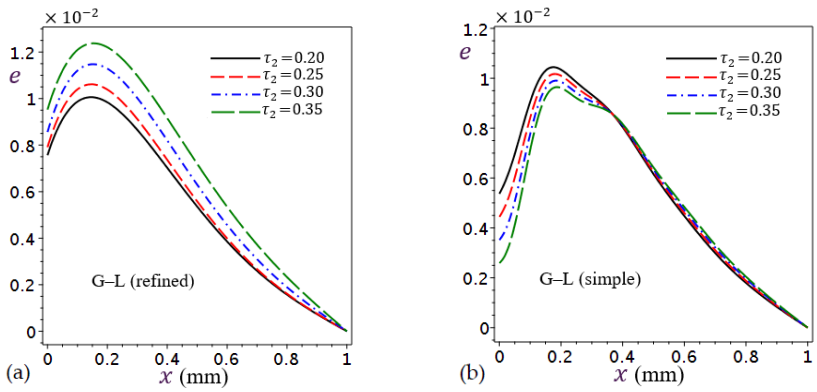

Fig. 14: Effect of second relaxation time τ_2 on dilatation e under harmonic heating (a) refined G–L theory and (b) simple G–L theory.

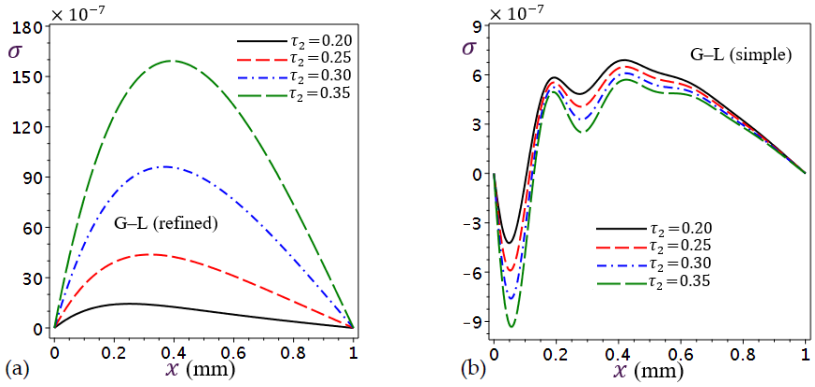

Fig. 15: Effect of second relaxation time τ_2 on stress σ under harmonic heating (a) refined G–L theory and (b) simple G–L theory.

To figure out how the blood perfusion rate w_b [46] effects on the different distributions consider that the time is $t = 10$ s, the angular frequency parameter is $\omega = 0.86$ rad s^{-1}, with relaxation times $\tau_1 = 0.1$ s, $\tau_2 = 0.14$ s. Table 3 shows the effect of the blood perfusion w_b on the distributions of temperature $\tilde{\theta} \equiv \theta \times 10^{-2}$, displacement $\tilde{u} \equiv u \times 10^6$, dilatation, $\tilde{e} \equiv e \times 10^2$ and stress $\tilde{\sigma} \equiv \sigma \times 10^6$ in the CTE theory, the L–S theory, the simple G–L theory, and different higher-order refined G–L theory at the position $x = 0.5$ mm where $\tilde{w}_b \equiv w_b \times 10^3$. The table demonstrates that across all theories, the values of the four variables decrease as w_b increases.

Table 3: Effect of blood perfusion w_b indifferent thermoelastic theories under harmonic heating.

	$\tilde{w}_b$	CTE	L–S	Simple G–L	Refined G–L	
				$N = 1$	$N = 2$	$N = 3$
$\tilde{\theta}$	1.00	0.168555	0.170953	0.170974	0.168312	0.167419
	1.87	0.168504	0.170909	0.170950	0.168259	0.167367
	3.87	0.168388	0.170806	0.170893	0.168135	0.167247
$\tilde{u}$	1.00	0.834960	0.869513	0.836875	0.779717	0.785431
	1.87	0.834607	0.869136	0.836496	0.779372	0.785087
	3.87	0.833796	0.868268	0.835627	0.778581	0.784298
$\tilde{e}$	1.00	0.479731	0.486557	0.538602	0.519113	0.510770
	1.87	0.479588	0.486431	0.538453	0.518893	0.510555
	3.87	0.479256	0.486139	0.538109	0.518384	0.510058
$\tilde{\sigma}$	1.00	0.620938	0.736144	0.638544	-0.192973	0.596579
	1.87	0.620781	0.736005	0.638383	-0.193224	0.596461
	3.87	0.620416	0.735683	0.638009	-0.193804	0.596187

As depicted in Fig. 16, three alternative values of the thermal conductivity k_t [47] are chosen to represent the distributions of temperature θ in the four theories of thermoelasticity to determine k_t effects. The temperature distributions in the refined G–L theory are affected by the different thermal conductivity values of the tissue k_t in a similar way to those in the remaining three models (CTE, simple G–L, L–S) where larger values of k_t give higher temperature curves.

The results are shown in Fig. 17 to clarify the distributions of temperature θ in different theories of thermoelasticity along the skin tissues over time from zero until after the passage of 15 seconds and relaxation times are taken by $\tau_1 = 0.1$ s, $\tau_2 = 0.14$ s and $\omega = 0.9$ rad s^{-1}. As the figure shows, the temperature values when applying harmonic heating to living tissues in the four models range between 75 K and -75 K, which is a periodic motion at the beginning of the biological tissue and decreases with the depth of the skin until it reaches zero at the end of the tissue, depending on the boundary condition of the issue under study, in which the temperature distribution differs according to refined G–L theory at the beginning of the tissue, where the curve takes a vibratory form at the beginning of time, and soon the shape of the curve stabilizes with the passage of a time and is similar to the rest of the distributions of other theories.

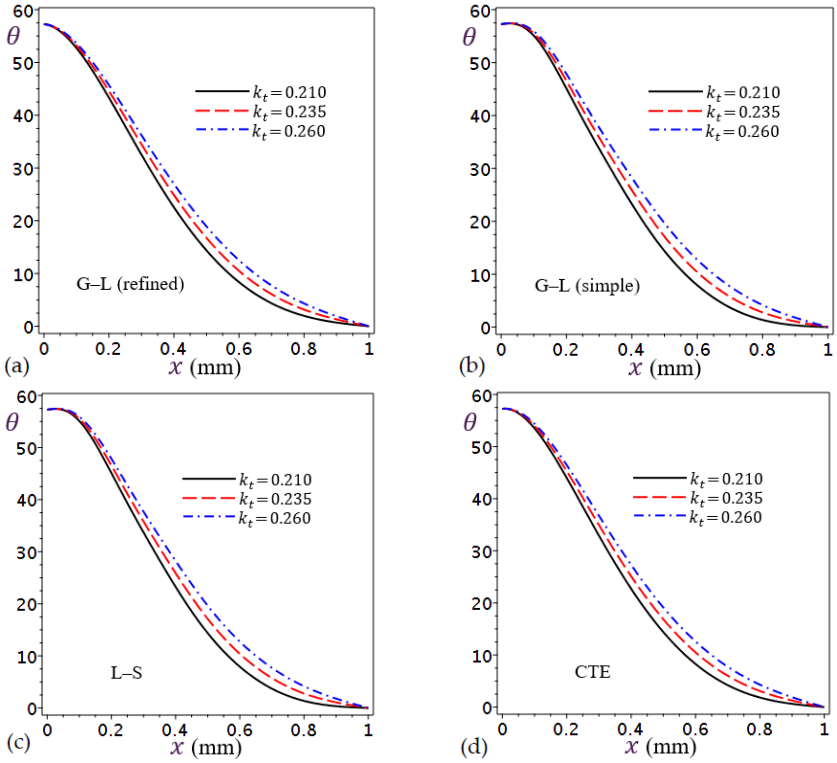

Fig. 16: Effect of thermal conductivity k_t on temperature θ under harmonic heating (a) refined G–L theory, (b) simple G–L theory, (c) L–S theory, and (d) CTE theory.

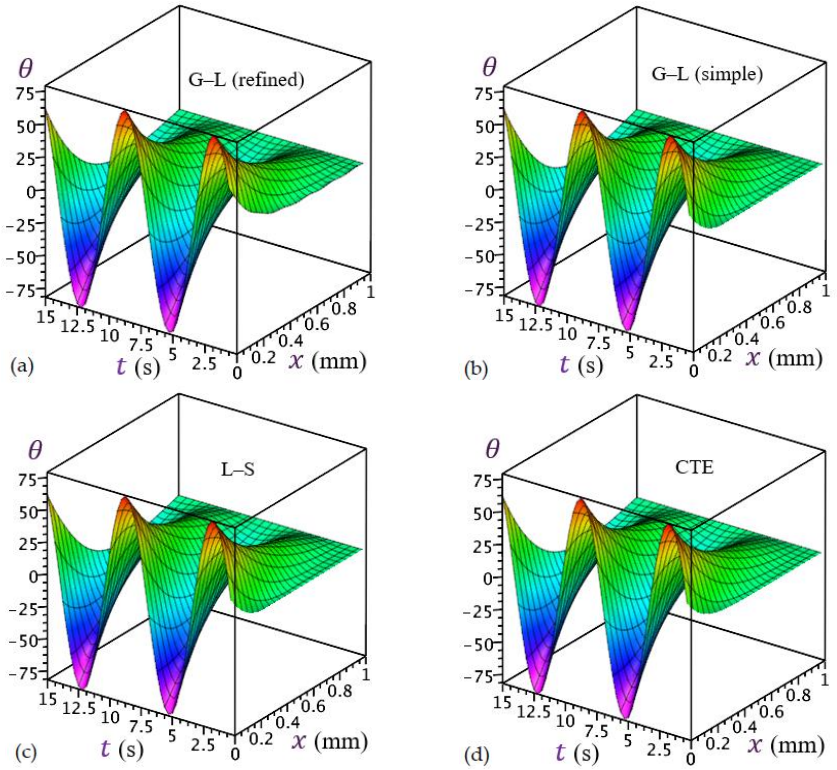

Fig. 17: 3D plots of temperature θ under harmonic heating along the x-axis of the skin tissue due to different theories of thermoelasticity (a) refined G–L theory, (b) simple G–L theory, (c) L–S theory, and (d) CTE theory.

7. Conclusions

The current article presents an analysis of the biothermal response of skin tissues in one dimension based on a refined Green–Lindsay theory of order three and compares it with the CTE theory, the L–S theory, and the simple G–L theory of thermoelasticity. The numerical solution, which includes the distributions of each of temperature θ, displacement u, strain e, and stress σ, has been shown graphically under the influence of harmonic heating on the outer surface of the skin. The temperature θ distributions resulting from the refined G–L theory are the lowest and had the same behavior as the rest of the heat curves resulting from the CTE theory, the L–S theory, and the simple G–L theory. Note that the displacement u curves resulting from the various theories of thermoelasticity had the same behavior and are close to each other. The dilatation e resulting from the refined G–L theory became the least. The stress σ curve resulting from the refined G–L theory is greater stress, but it falls in the same range as the remaining stress curves of other theories.

On the subject of angular frequency parameter ω, the temperature θ is affected in the refined G–L theory in the same way in the (CTE, L–S, and simple G–L) theories, the effect is summarized in that the smaller the value of ω, the higher the temperature at the outer surface of the skin and then decreases through the depth, and the greater ω, the lower the temperature on the outer surface and the curve convexed through the depth of the skin and then begins to descend until it reaches the inner surface and is equal to zero. The different ω values showed different displacement distributions, whereas with the decrease in ω the displacement curve became more convex. The dilatation distributions in the refined G–L theory are affected by changing the ω values in a pattern similar to the (CTE, L–S, and simple G–L) theories, noting that the refined G–L theory gives the highest dilatation at the outer surface of the skin, and an increase in ω gives greater stress and smaller ω values affect the stress curve more in the refined G–L theory.

The effect of different relaxation times is also studied, an increase in τ_1 raises the temperature θ, an increase in τ_1 gives a wavy displacement u curve, and dilatation e. The lowest value of τ_1 gave the highest stress σ. An increase in τ_2 decreases the temperature θ, The increase in τ_2 gave a regular decrease in the displacement u curves in the first half of the tissue, then the curves intersect and the effect is reversed. An increase in τ_2 gives a higher dilatation e. An increase in τ_2 gives higher stress σ.

Some biological parameters such as blood perfusion w_b and thermal conductivity k_t of the skin have also been studied. The increase in perfusion of blood w_b gives a decrease in temperature θ, displacement u, strain e, and stress σ. An increase in the skin's thermal conductivity k_t raises the temperature θ. Possible of increasing the time and its effect has been discussed, with time, the outer surface is affected more than the rest of the biological tissue by harmonic heating, and the temperature θ takes the form of waves, and the waves begin to descend through the depth of the tissue until they reach zero at the inner surface.

References

[1] H. H. Pennes, Analysis of Tissue and Arterial Blood Temperatures in the Resting Human Forearm, *Journal of Applied Physiology,* Vol. 85, No. 1, pp. 5-34, 1998.

[2] C. Cattaneo, A Form of Heat-Conduction Equations Which Eliminates the Paradox of Instantaneous Propagation, *Comptes Rendus,* Vol. 247, pp. 431, 1958, 1958.

[3] P. Vernotte, Les paradoxes de la theorie continue de l'equation de la chaleur, *Compt. Rendu,* Vol. 246, pp. 3154-3155, 1958, 1958.

[4] D. Y. Tzou, The generalized lagging response in small-scale and high-rate heating, *International Journal of Heat and Mass Transfer,* Vol. 38, No. 17, pp. 3231-3240, 1995/11/01/, 1995.

[5] S. Wahyudi, F. Gapsari, Analysis of Temperature Distribution of Human Skin Tissue in Various Environmental Temperature with the Finite Volume Method, *International Journal of Mechanical Engineering and Robotics Research*, pp. 99-105, 01/01, 2022.

[6] S. K R, I. Ramarao, D. P.A, BIOHEAT TRANSFER EQUATION WITH TRANSIENT HEAT FLUX CONDITIONS TO SKIN TISSUE AN ANALYTICAL APPROACH, *International Journal of Pure and Applied Mathematics,* Vol. 120, pp. 871-879, 01/01, 2018.

[7] I. Kaur, P. Lata, K. S. Handa, Effects of Memory Dependent Derivative of Bio-heat Model in Skin Tissue exposed to Laser Radiation, *EAI Endorsed Transactions on Pervasive Health and Technology,* Vol. 6, pp. 164589, 07/13, 2018.

[8] M. B. Bera, M. Mondal, B. S. Mahapatra, G. Roymahapatra, P. Acharjya, Generalized theory of thermoelasticity in isotropic and homogenious thermoelastic solids, *Turkish Journal of Computer and Mathematics Education (TURCOMAT),* Vol. 11, No. 3, pp. 1877-1885, 2020.

[9] G. Oguntala, Y. Hu, G. Sobamowo, 2021, *Computational Modelling of Dual-Phase Lag Bioheat Process in Cooling of Cutaneous Tissue Exposed to High Heating for Burn Injury Prediction*,

[10] S. Ozen, S. Helhel, O. Cerezci, Heat analysis of biological tissue exposed to microwave by using thermal wave model of bio-heat transfer (TWMBT), *Burns : journal of the International Society for Burn Injuries,* Vol. 34, pp. 45-9, 03/01, 2008.

[11] I. Abbas, A. Abdalla, F. Anwar, H. Sapoor, A numerical solution of 2-D single-phase-lag (SPL) bio-heat model using alternating direction implicit (ADI) finite difference method, *Sohag Journal of Sciences,* Vol. 7, No. 3, pp. 131-141, 2022.

[12] M. Paruch, B. Mochnacki, Cattaneo-Vernotte bio-heat transfer equation. Identificaton of external heat flux and relaxation time in domain of heated skin tissue, *Computer Assisted Mechanics and Engineering Sciences,* Vol. 25, pp. 71-80, 2018.

[13] S. K. Sharma, D. Kumar, A Study on Non-Linear DPL Model for Describing Heat Transfer in Skin Tissue during Hyperthermia Treatment, *Entropy,* Vol. 22, No. 4, pp. 481, 2020.

[14] P. H. Ziaei, H. Moosavi, A. A. Moradi, Analysis of the dual phase lag bio-heat transfer equation with constant and time-dependent heat flux conditions on skin surface, *Thermal Science,* Vol. 20, pp. 1457-1472, 2016.

[15] M. Ezzat, Bio-thermo-mechanics behavior in living viscoelastic tissue under the fractional dual-phase-lag theory, *Archive of Applied Mechanics,* Vol. 91, 09/01, 2021.

[16] R. Kumar, R. Tiwari, A. Singhal, S. Mondal, Characterization of thermal damage of skin tissue subjected to moving heat source in the purview of dual phase lag theory with memory-dependent derivative, *Waves in Random and Complex Media*, 09/29, 2021.

[17] Y. Hu, X. Zhang, X.-F. Li, Thermoelastic response of skin using time-fractional dual-phase-lag bioheat heat transfer equation, *Journal of Thermal Stresses,* Vol. 45, pp. 597-615, 06/06, 2022.

[18] J. Zhou, J. K. Chen, Y. Zhang, Dual-Phase Lag Effects on Thermal Damage to Biological Tissues Caused By Laser Irradiation, *Computers in biology and medicine,* Vol. 39, pp. 286-93, 03/01, 2009.

[19] D. Kumar, S. Singh, K. Rai, Analysis of Classical Fourier, SPL and DPL Heat Transfer Model in Biological Tissues in Presence of Metabolic and External heat source, *Heat and Mass Transfer Springer,* Vol. 52, 06/24, 2015.

[20] R. Kumar, A. K. Vashisth, S. Ghangas, Analytical solution of bioheat transfer equation with variable thermal conductivity in skin, in *Proceeding of*.

[21] R. Fazlali, H. Ahmadikia, Analytical solution of thermal wave models on skin tissue under arbitrary periodic boundary conditions, *International Journal of Thermophysics,* Vol. 34, pp. 139-159, 2013.

[22] P. Forghani, H. Ahmadikia, A. Karimipour, Non-Fourier Boundary Conditions Effects on the Skin Tissue Temperature Response, *Heat Transfer—Asian Research,* Vol. 46, No. 1, pp. 29-48, 2017.

[23] M. A. Biot, Thermoelasticity and irreversible thermodynamics, *Journal of applied physics,* Vol. 27, No. 3, pp. 240-253, 1956.

[24] H. W. Lord, Y. Shulman, A generalized dynamical theory of thermoelasticity, *Journal of the Mechanics and Physics of Solids,* Vol. 15, No. 5, pp. 299-309, 1967.

[25] A. E. Green, K. Lindsay, Thermoelasticity, *Journal of elasticity,* Vol. 2, No. 1, pp. 1-7, 1972.

[26] A. Green, P. Naghdi, Thermoelasticity without energy dissipation, *Journal of elasticity,* Vol. 31, No. 3, pp. 189-208, 1993.

[27] A. Bagri, M. R. Eslami, Analysis of Thermoelastic Waves in Functionally Graded Hollow Spheres Based on the Green-Lindsay Theory, *Journal of Thermal Stresses,* Vol. 30, No. 12, pp. 1175-1193, 2007/10/30, 2007.

[28] A. Pramanik, S. Biswas, 2020, *Eigenvalue approach to hyperbolic thermoelastic problem in porous orthotropic medium with Green- Lindsay model*,

[29] S. Abo-Dahab, Green Lindsay Model on Propagation of Surface Waves in Magneto-Thermoelastic Materials with Voids and Initial Stress, *Journal of Computational and Theoretical Nanoscience, vol. 11, issue 3, pp. 763-771,* Vol. 11, pp. 763-771, 03/01, 2014.

[30] A. Kumar, O. N. Shivay, S. Mukhopadhyay, Infinite speed behavior of two-temperature Green–Lindsay thermoelasticity theory under temperature-dependent thermal conductivity, *Zeitschrift für angewandte Mathematik und Physik,* Vol. 70, 01/02, 2019.

[31] N. Sarkar, S. De, N. Sarkar, Modified Green–Lindsay model on the reflection and propagation of thermoelastic plane waves at an isothermal stress-free surface, *Indian Journal of Physics,* Vol. 94, pp. 1215-1225, 08/08, 2020.

[32] S. R. Choudhuri, On a thermoelastic three-phase-lag model, *Journal of Thermal Stresses,* Vol. 30, No. 3, pp. 231-238, 2007.

[33] A. Hobiny, F. Alzahrani, I. Abbas, Analytical Estimation of Temperature in Living Tissues Using the TPL Bioheat Model with Experimental Verification, *Mathematics,* Vol. 8, pp. 1188, 07/19, 2020.

[34] A. M. Zenkour, T. Saeed, A. A. Al-Raezah, A 1D thermoelastic response of skin tissue due to ramp-type heating via a fractional-order Lord–Shulman model, *Journal of Computational Applied Mechanics*, Vol. 54, No. 3, pp. 365-377, 2023.
[35] M. Sobhy, A. Zenkour, Refined Lord–Shulman Theory for 1D Response of Skin Tissue under Ramp-Type Heat, *Materials*, Vol. 15, pp. 6292, 09/10, 2022.
[36] A. Zenkour, T. Saeed, K. Alnefaie, Refined Green–Lindsay Model for the Response of Skin Tissue under a Ramp-Type Heating, *Mathematics*, Vol. 11, pp. 1437, 03/16, 2023.
[37] A. Zenkour, T. Saeed, A. Aati, Refined Dual-Phase-Lag Theory for the 1D Behavior of Skin Tissue under Ramp-Type Heating, *Materials*, Vol. 16, pp. 2421, 03/17, 2023.
[38] A. M. Zenkour, T. Saeed, A. M. Aati, Analyzing the Thermoelastic Responses of Biological Tissue Exposed to Thermal Shock Utilizing a Three-Phase Lag Theory, *Journal of Computational Applied Mechanics*, 2023.
[39] M. Aljadani, A. Zenkour, A Modified Two-Relaxation Thermoelastic Model for a Thermal Shock of Rotating Infinite Medium, *Materials*, Vol. 15, pp. 9056, 12/18, 2022.
[40] A. M. Zenkour, Exact coupled solution for photothermal semiconducting beams using a refined multi-phase-lag theory, *Optics & Laser Technology*, Vol. 128, pp. 106233, 2020/08/01/, 2020.
[41] A. M. Zenkour, H. F. El-Mekawy, On a multi-phase-lag model of coupled thermoelasticity, *International Communications in Heat and Mass Transfer*, Vol. 116, pp. 104722, 2020/07/01/, 2020.
[42] A. M. Zenkour, On Generalized Three-Phase-Lag Models in Photo-Thermoelasticity, *International Journal of Applied Mechanics*, Vol. 14, No. 02, pp. 2250005, 2022.
[43] A. M. Zenkour, Thermal diffusion of an unbounded solid with a spherical cavity via refined three-phase-lag Green–Naghdi models, *Indian Journal of Physics*, Vol. 96, No. 4, pp. 1087-1104, 2022/03/01, 2022.
[44] D. Y. Tzou, Experimental support for the lagging behavior in heat propagation, *Journal of Thermophysics and Heat Transfer*, Vol. 9, No. 4, pp. 686-693, 1995.
[45] G. Honig, U. Hirdes, A method for the numerical inversion of Laplace transforms, *Journal of Computational and Applied Mathematics*, Vol. 10, No. 1, pp. 113-132, 1984.
[46] Q. Zhang, Y. Sun, J. Yang, Bio-heat response of skin tissue based on three-phase-lag model, *Scientific Reports*, Vol. 10, No. 1, pp. 16421, 2020.
[47] T. Okabe, T. Fujimura, J. Okajima, S. Aiba, S. Maruyama, Non-invasive measurement of effective thermal conductivity of human skin with a guard-heated thermistor probe, *International Journal of Heat and Mass Transfer*, Vol. 126, pp. 625-635, 11/01, 2018.